CCA-759

541.135:546.47
Conference Paper

The Electrocrystallization of Metals. Investigation of Zinc*

*D. M. Dražić, S. Hadži Jordanov,** and Z. Nagy****

Faculty of Technology and Metallurgy, University of Belgrade, 11000 Belgrade, Serbia, Yugoslavia

Received December 11, 1972

In electrodeposition of zinc depending on the condition of deposition, various effects of electrocrystallization can be observed.

In acid solution of zinc sulfate the considerable surface diffusion overpotential appears at lower values of the total overpotential, indicating the surface diffusion of adions as the rate determining step. An interesting dependence of exchange current density on pH with a minimum at pH ~ 2 indicate the probable change in structure of the reacting particle. The mechanism of the reaction is evaluated.

In alkaline zincate solutions no surface diffusion limitations can be detected. However, due to the rather low zincate ion concentration and high exchange current density zinc deposition proceeds practically always under the diffusion control.

Morphology of zinc deposited depends considerably on the value of the electrode potential. This can be seen from the experiments in which the deposition morphology was observed with a scanning electron microscope. It was found possible to disrupt the deposition repeatedly for microscopic observation and than continue deposition. At low overpotentials (up to 50 mV) epitaxial layer type growth was observed with the linear increase of the microstep width with time. For this effect a theory is proposed which accounts also for the observed effects of substrate orientation.

At larger overpotentials (50—100 mV) boulder type deposit was observed, most of which were not epitaxial with the substrate. They are suggested to be originated by nucleation. The boulder density per cm^2 is first sharply increasing, and then slowly decreasing with time. A statistical calculation for this is given based on the model that large boulders consume the smaller ones. With further deposition a small fraction of the boulders develop into dendrites, their number being limited by the available total current.

INTRODUCTION

The electrodeposition and electrosrystallization of zinc represents an interesting and complex problem where one encounters many electrochemical phenomena combined together in one system.. Obviously, this does not make things easier for studying each phenomenon in great detail. However, the electrochemistry of zinc in acid solutions as used in the zinc electrowinning process, as well as in alkaline solutions, as used in batteries, needs better

---

* Based on a lecture presented at the *III International Summer School on the Chemistry of Solid/Liquid Interfaces,* Rovinj, Yugoslavia, July 1—5, 1972.

** Present address: Faculty of Technology and Metallurgy, University of Skopje, 91000 Skopje, Macedonia, Yugoslavia.

*** Present address: Diamond Shamrock Chemical Co. Divisional Technical Center, Painesville, Ohio, 44077, U.S.A.

understanding and a thorough analysis of all the aspects of the processes involved.

In this paper we shall limit ourselves to the discussion of two special cases each one serving as an ilustration of the complexity of the phenomena involved: *a)* The elucidation of the reaction mechanism for electrodeposition and dissolution of zinc from acid zinc sulfate solutions, and *b)* The effects of the experimental conditions during the electrodeposition of zinc from the alkaline zincate solutions on the morphology of the deposit.

Electrodeposition and Dissolution of Zinc from Acid Sulfate Solution

The kinetics and mechanism of the deposition and dissolution of zinc have been investigated by many authors during the last two decades. They have been done with zinc amalgams and solid zinc electrodes in all pH ranges from acid to alkaline, and in the presence of various anions including those forming stable complexes with zinc ions. A more detailed review of the relevant literature is given elsewhere[1-2]. The results published, particularly for the acid pH region differ in many respects, and in some cases seam to be contradictory. For example, Kravcov and Zverevich[3] suggest a two electron exchange mechanism ($Zn^{2+} + 2\,e \rightleftharpoons Zn$), Losev and Budev[4] suggest two stepwise one electron reactions with Zn^{+} as the intermediate, Lorenz[5] concludes that the reaction proceeds with the two-electron exchange, and the formation of Zn adions, the surface diffusion of those being the rate determining step, while some authors suggest the mechanisms with simultaneous or stepwise electron exchange reactions with even more than two electrons[6,7].

The process of zinc deposition is always accompanied by hydrogen evolution, due to the electronegativity of zinc in respect to hydrogen ions and one of the possible reasons for the differences in the experimentally obtained data could be the negligence of those factors, otherwise shown[8,9] to be of importance in the interpretation of the mechanisms for some other electronegative metals (*e. g.*, Fe, Ni, Co). The complexing of Zn^{2+} ions with anions present in the solution could be an additional effect of importance in this analysis as well.

Due to the rather high exchange current density the open circuit or corrosion potential* of zinc in zinc sulfate solutions at low H^{+} ion concentration ($pH > 3$) is close to the reversible zinc electrode potential. However, when the corrosion of the zinc rod electrode was measured[10] in lower pH regions up to $pH = 0.5$, the rather complex and unusual S-shaped dependence of the corrosion potential *vs.* pH was obtained as shown in Fig. 1. The upper part of the curve approaching the reversible Zn potential obviously indicates that the hydrogen evolution current, *i. e.* the corrosion current, becomes smaller than the Zn exchange current, hence, the corrosion potential is close to the reversible one. On the other hand, the lower part of the diagram indicates some deviation of the anodic process in the low pH region from the one occurring in the solutions with the pH values larger than 2.

The anodic polarization curves obtained galvanostatically[11] with zinc rod electrodes in the solutions containing various concentrations of $ZnSO_4$ and Na_2SO_4 to make the total ionic strength about 4, are shown in Fig. 2 for one set of measurements at various pH (0.5—5). Most of the curves have a well-

* All the potentials in this paper are referred to the standard hydrogen electrode.

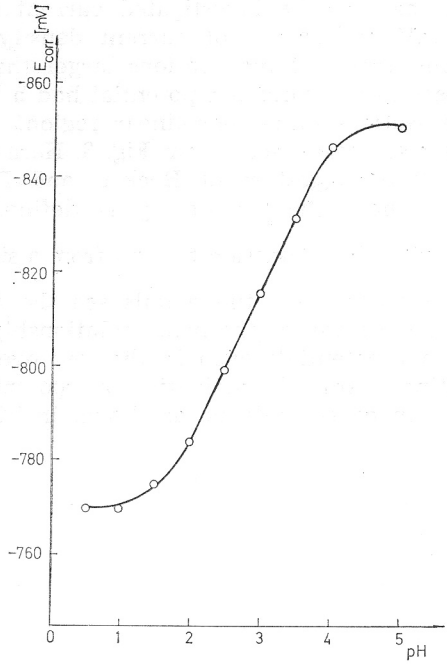

Fig. 1. Corrosion potentials of zinc as a function of solution pH ($C_{Zn^{+2}}$ = 0.01 M).

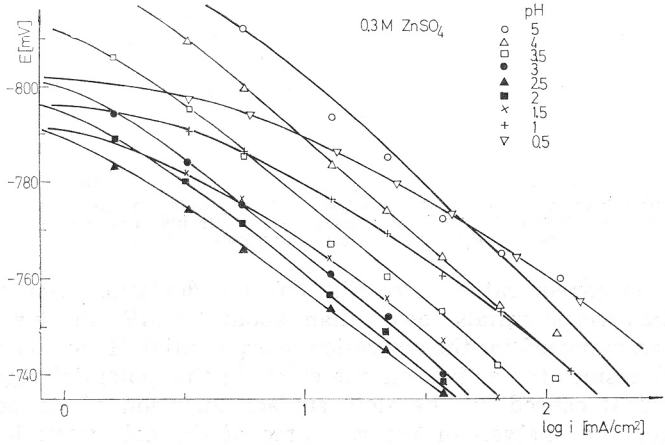

Fig. 2. Anodic polarization curves at various pH of the solution.

expressed linear Tafel part in the investigated current density region with a slope of about 40 mV per decade of current density. However, for the solutions containing Zn^{2+} ions in concentrations larger than 0.3 M, the initial part of the curves closer to the corrosion potential had a longer curved shape than expected for the Butler-Volmer non-linear region.

This effect can be more easily seen from Fig. 3. Here instead of the usual η-log i plot, following the suggestion of Bockris and Despić[12], the similar η-log y plot is given, where the function y is defined as $y = i/[1 - \exp\left(\frac{zF}{RT}\eta\right)]$. The definition of the y function follows from a simple transformation of the Butler-Volmer equation (for the details see the original paper), and when plotted in a η — log y diagram, the lienar relationship should be obtained in the whole span of overpotentials even in the low overpotential region, if the overpotential existing is only the activation overpotential. This was really obtained for low Zn^{2+} ion concentrations, as shown in Fig. 3a. However, for

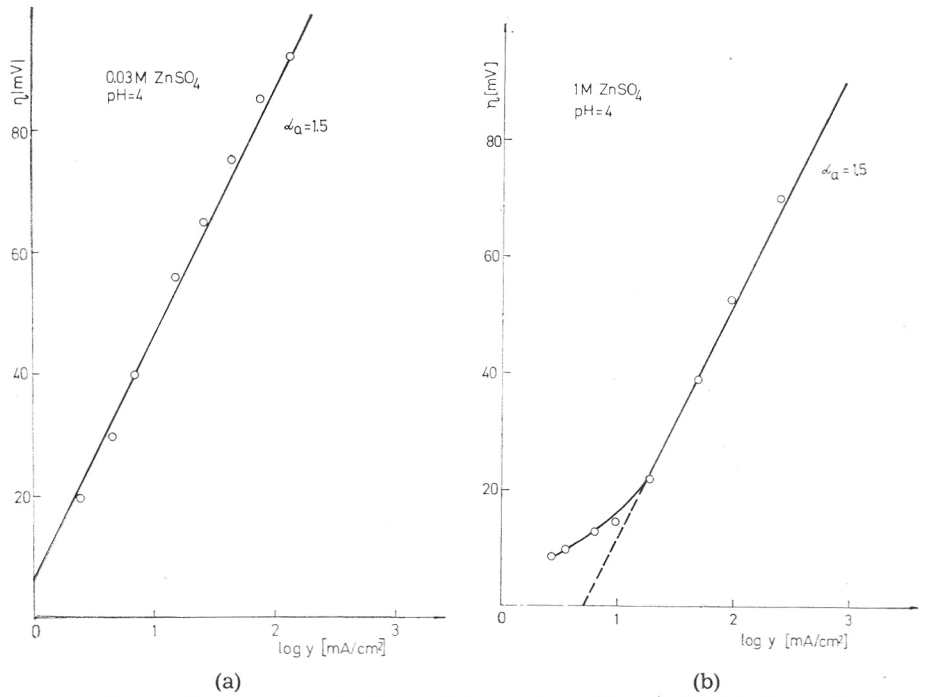

Fig. 3. Anodic polarization curves in the modified η — log$y$ diagram (for detail see the text) at pH = 4; *a)* for 0.01 M $ZnSO_4$; *b)* for 1 M $ZnSO_4$; — — — Broken line represents the expected relationship for activation overpotential only.

higher Zn^{2+} ion concentrations (see Fig. 3b), the deviation from the linearity exists for the overpotentials lower than about 30 mV. In this region they are larger than expected for the activation overpotential. Hence, some additional overpotential besides the activation one exists in this potential region, possibly the overpotential caused by the slow surface diffusion of Zn adions at the metal surface. The analysis of the rise time of the galvanostatic transients[10] following the method of Bockris and Mehl[13] indicates the considerable surface

diffusion overpotentials in this region too. Hence, the sometimes reported values of Tafel slope for the anodic polarization curves lower than 40 mV could be ascribed to the situations where besides the activation the surface diffusion overpotential existed, distorting considerably the polarization curves and hence the value of the Tafel slope.

Another important conclusion following from the data presented in Fig. 2 is the complex dependence of the rate of the anodic process on the pH of the solution. This can be seen better from Fig. 4 where the current densities at

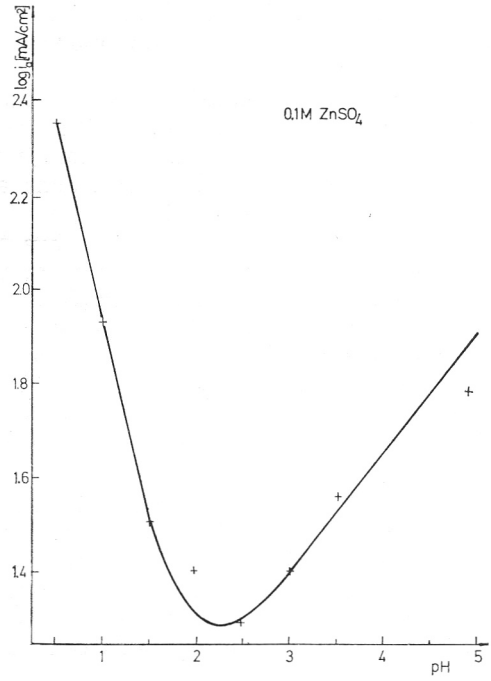

Fig. 4. Plot of the logarithm of anodic current density at — 760 mV *versus* pH. First slope: — 0.8; second slope: + 0.25.

the constant potential of — 760 mV are plotted versus the pH of the solutions. The first previously unreported fact is that the pH affects the rate of the anodic process. The second one is that for pH's lower than about 2 increase of H^+ ion concentration accelerates the dissolution reaction with the slope, *i. e.*, the reaction order for H^+ ions is $\partial \log i/\partial \text{pH} \approx 0.8$, while for pH's higher than 2, effect is the reverse, the decrease of H^+ ion concentration accelerates the reaction with an apparent reaction order $\partial \log i/\partial \text{pH} \approx 0.25$.

A) The experimental anodic polarization data can be expressed analytically by the relation

$$i_a = k_1 \cdot C_{H^+}^{0.8} \exp\left(\frac{\alpha_a F}{RT} E\right) \tag{1}$$

for pH $<$ 2, and

$$i_a = k_2 \cdot C_{OH^-}^{0.25} \exp\left(\frac{\alpha_a F}{RT} E\right) \quad (2)$$

for pH $>$ 2, the anodic transfer coefficient α_a having the value 1.5.

The reasons for such behavior are not clear as yet. The direct participation of H^+ or OH^- ions in the formation of the activated complex does not seem to be the real case for two reasons. Firstly, the mechanisms in the two indicated pH regions should be quite different. Secondly, the reaction orders as determined experimentally would indicate participation of more than one Zn ion particle in the formation of the activated complex; in the case of OH^- ions even 4 Zn^{2+} ions with one OH^- ion. Both assumptions do not seem justified from the kinetic point of view.

The pH effect observed could be related also to the change of the structure of anions if anions form any kind of complexes with Zn^{2+} ions. Namely, two facts are known. Firstly, the second dissociation constant of sulfuric acid[14] is about 10^{-2}, indicating that below pH 2, most anions are in HSO_4^- form, while above that pH they are in the form of the simple SO_4^{2-} ions. Secondly, Zn^{2+} and SO_4^{2-} ions are known to form ion pairs with a stability constant of about 200[15]. Hence, the increase of the reaction rate in the pH range 2—4 could be related to the change in the concentration of simple SO_4^{2-} ions, the increase of the concentration of ion-paired $Zn \cdot SO_4$ particles and decrease of the activation energy for the anodic process due to the decrease of the ground state energy of the complexed particle. However the effect at pH lower than 2 cannot be explained by this argument. More detailed experimental work in this pH region should be done before a proper analysis of the phenomenon can be made.

B) The analysis of the stationary cathodic polarization curves presented in Fig. 5 is complex too. Firstly, the experimentally measured cathodic currents are always the sums of zinc deposition and hydrogen evolution currents, and only in the case when hydrogen evolution current is negligible compared to the zinc deposition current (as in the case of higher pH values), the experimentally measured values shown in the diagrams can be approximated with

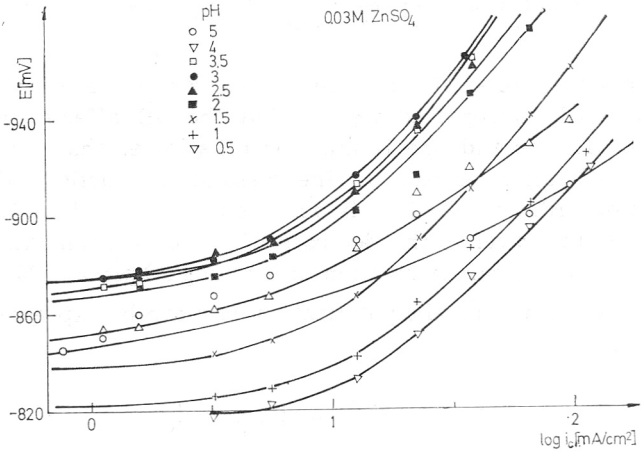

Fig. 5. Cathodic polarization curves at various pH of the solution.

the latter one. Secondly, as shown elsewhere[8], if the primary zinc deposition and dissolution process is pH dependent (as shown before to be the case), and hydrogen codeposition is under diffusion control affecting the real pH at the electrode surface, the cathodic polarization curve and its Tafel slope should deviate from the normally expected values.

Hence, before the analysis of the cathodic polarization curves a separate analyzis of the hydrogen evolution itself should be made. The results of such measurements in Zn^{2+} ion-free solution of different pH values are given in Fig. 6a as the stationary state polarization curves and in Fig. 6b if only the values of the activation overpotentials are taken from the galvanostatic transients.

In the latter case, Tafel lines with 120 mV slopes and reaction order of $\partial \log i/\partial \log C_{H^+} = 1$ were obtained proving the H^+ ion discharge to be the cathodic process. However, the stationary state curves presented in Fig. 6a clearly show the existence of considerable concentration polarization in respect to H^+ ions and even the appearance of the limiting diffusion hydrogen evolution current for higher pH's in the range of the potential of zinc deposition.

The cathodic polarization curves shown in Fig. 5 exhibit the linear Tafel regions with the slopes of about 120 mV for pH's lower than about 3, while for higher values the slopes become smaller going down to *ca.* 80 mV for the highest pH measured. The position of the lines in the diagram depends on the actual pH of the solution. At a constant potential the total cathodic current decreases up to about pH = 3, and therafter starts increasing again.

This diagram can be interpreted in the following manner if one compares it with the hydrogen evolution curves from Fig. 6. At lower pH values the

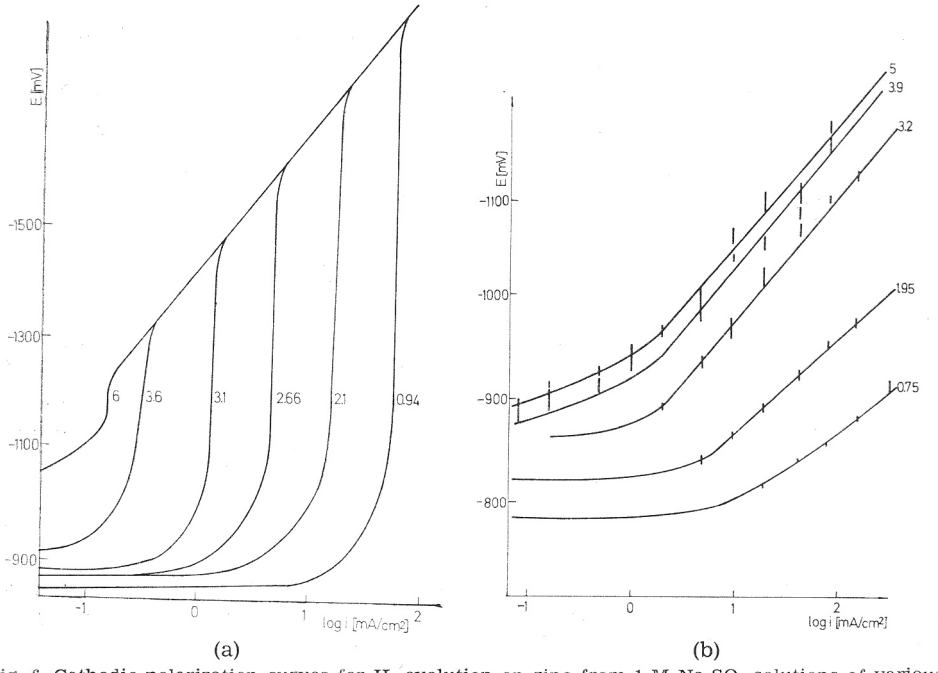

Fig. 6. Cathodic polarization curves for H_2 evolution on zinc from 1 M Na_2SO_4 solutions of various pH: *a)* Stationary state measurements; *b)* Galvanostatic measurements of activation overpotentials only.

experimental points represent the sum of zinc deposition and hydrogen evolution, the latter one being the dominant contribution. With the increase of pH the codeposition current decreases (see Fig. 6), and hence the total current decreases as well.

The constant slope of 120 mV indicates that both the cathodic processes (*i. e.*, Zn deposition and H_2 evolution) proceed with the same slope of 120 mV. For pH's higher than about 3, the hydrogen evolution reaction is under diffusion control and the pH at the electrode surface is not any more like that in the bulk.

It has been shown elsewhere[8] that the surface H^+ ion concentration, $(C_{H^+})_s$ can be related to the bulk H^+ ion concentration, $(C_{H^+})_b$ (when the concentration polarization, E is considerable and taken as the negative value), by the expression

$$(C_{H^+})_s = (C_{H^+})_b \exp\left(\frac{0.5\,F}{RT}\,E\right) \tag{3}$$

or for OH^- ions

$$(C_{OH^-})_s = (C_{OH^-})_b \exp\left(-\frac{0.5\,F}{RT}\,E\right) \tag{4}$$

rather than by the simple Nernst-type relation as often done by many authors. The basic reason for introducing the correction factor 0.5 (or more precisely the symmetry factor β, which is for H_2 evolution about 0.5) is that, due to the low exchange current densities for H_3 evolution (for Zn it is about 10^{-8} A/cm^2) the total polarization in the limiting current region is always the sum of the activation and concentration overpotentials. Hence, the decrease of H^+ ion concentration increases the nominal Nernst-type concentration overpotential due to the change of the reversible potential, but also increases the actual activation overpotential by the same amount, through the effect of concentration on the exchange current density, i_0, for H_2 evolution[16] ($i_0 = k \cdot C_{H^+}^{0.5}$).

The cathodic current density, taking into account the »catalytic« effect of H^+ of OH^- ions proved in the anodic measurements for pH $>$ 2 can be given by the following equation

$$i_c = k_3 \cdot C_{Zn^{2+}} (C_{OH^-})_s^{0.25} \exp\left(-\frac{0.5\,F}{RT}\,E\right) \tag{5}$$

assuming that the first electron exchange step for Zn deposition is the rate determining (*i. e.*, $Zn^{2+} + e \rightarrow Zn^+$) and hence $\alpha_c = 0.5$[17].

The apparent current density — potential relation, accessible to the experimental test, when only the bulk pH can be kept constant, can be obtained by replacing equation (4) in equation (5). The resulting relation is

$$i_c = k \cdot C_{Zn^{2+}} (C_{OH^-})_b^{0.25} \exp\left(-\frac{0.62\,F}{RT}\,E\right) \tag{6}$$

from which the apparent Tafel slope of $RT/0.62\,F = 96$ mV can be calculated. Hence, the experimentally observed lowering of the cathodic Tafel slope values below 120 mV for pH's higher than 3 can be rationally explained by the pH dependency of the Zn deposition reaction and the surface pH change caused by the parallel diffusionally controlled H^+ ion discharge.

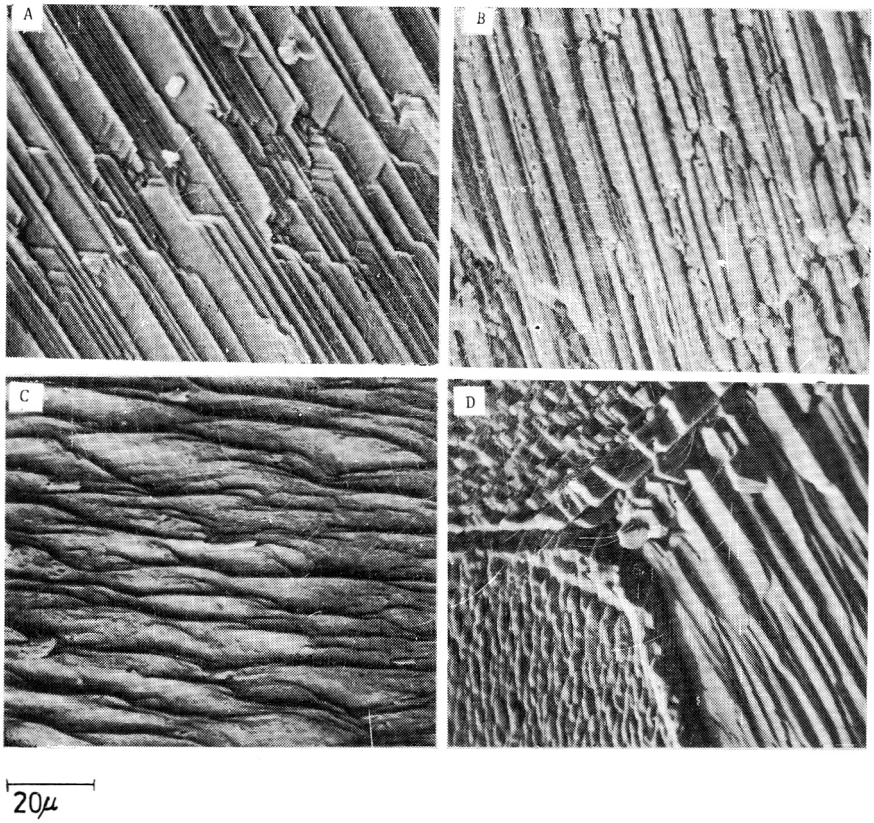

Fig. 7. Scanning electron microscope (SEM) pictures of zinc deposited at 50 mV for several electrode samples: *A*. Electrode No. 1., 16.5 C/cm²; *B*. Electrode No. 3., 11.5 C/cm²; *C*. Electrode No. 4., 14. C/cm²; *D*. Electrode No. 1., 20 C/cm².

[To face page 206]

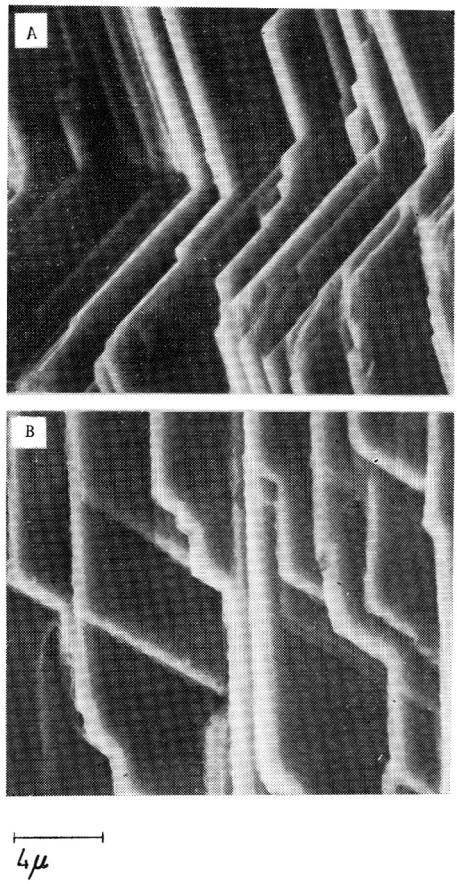

Fig. 8. SEM pictures of deposition at 50 mV. The »c« axis of substrate is aligned with the optical axis of the microscope: *A*. Electrode No. 4., 15 C/cm²; *B*. Electrode No. 1., 16.5 C/cm².

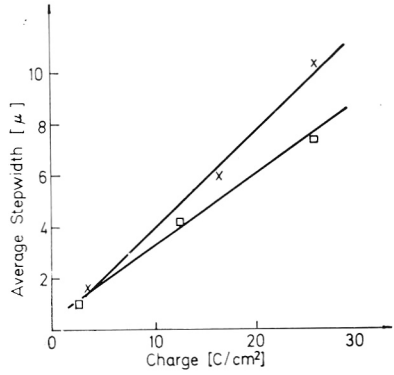

Fig. 9. Dependence of average stepwidth on charge; X — electrode No. 1; □ — electrode No. 3.

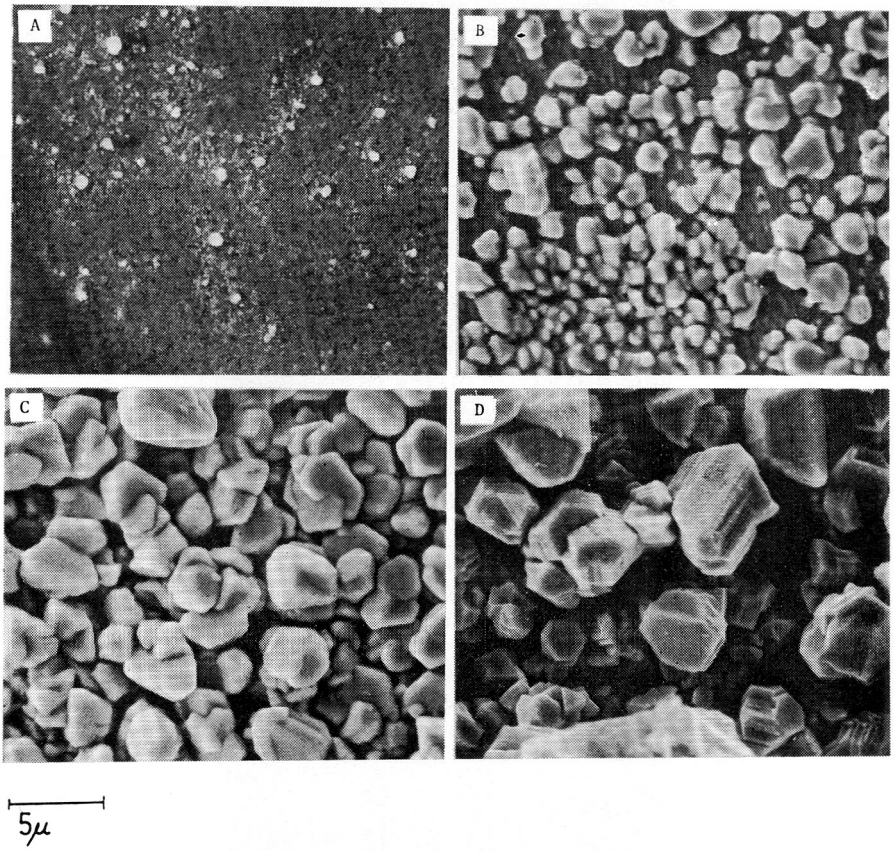

Fig. 10. SEM pictures of deposition at 100 mV as function of charge. Electrode No. 3: *A* — 0.3 C/cm²; *B* — 2.8 C/cm²; *C* — 9 C/cm²; *D* — 17 C/cm².

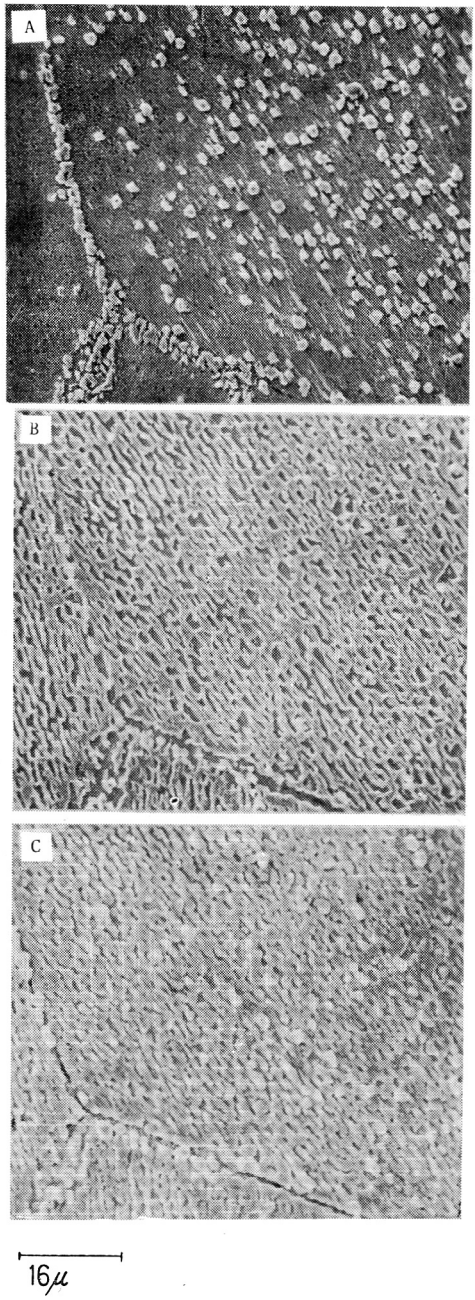

Fig. 11. SEM pictures from deposition — dissolution — deposition experiment: *A* — after deposition of 1.2 C/cm²; *B* — after dissolution of 0.3 C/cm²; *C* — after deposition of 1.4 C/cm².

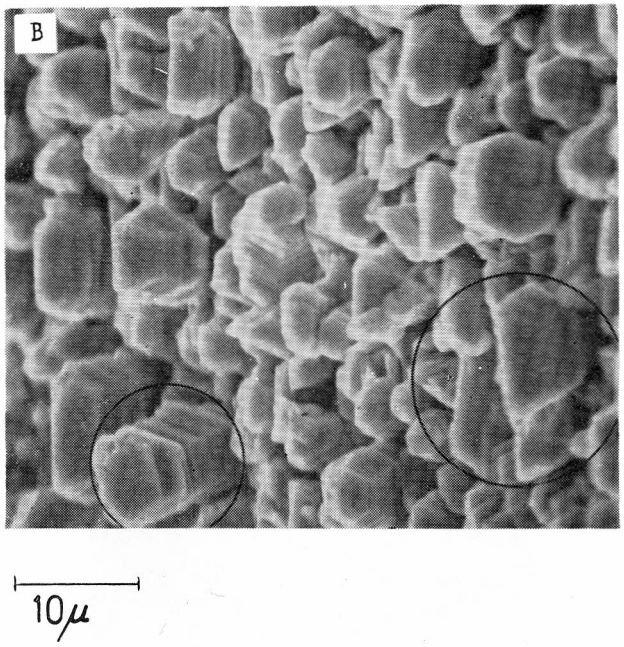

Fig. 12. SEM pictures of boulders obtained at 100 mV. The »c« axis is aligned with the optical axis of the microscope. Electrode No. 3. 16 C/cm². Boulders encircled are misaligned in respect to the substrate.

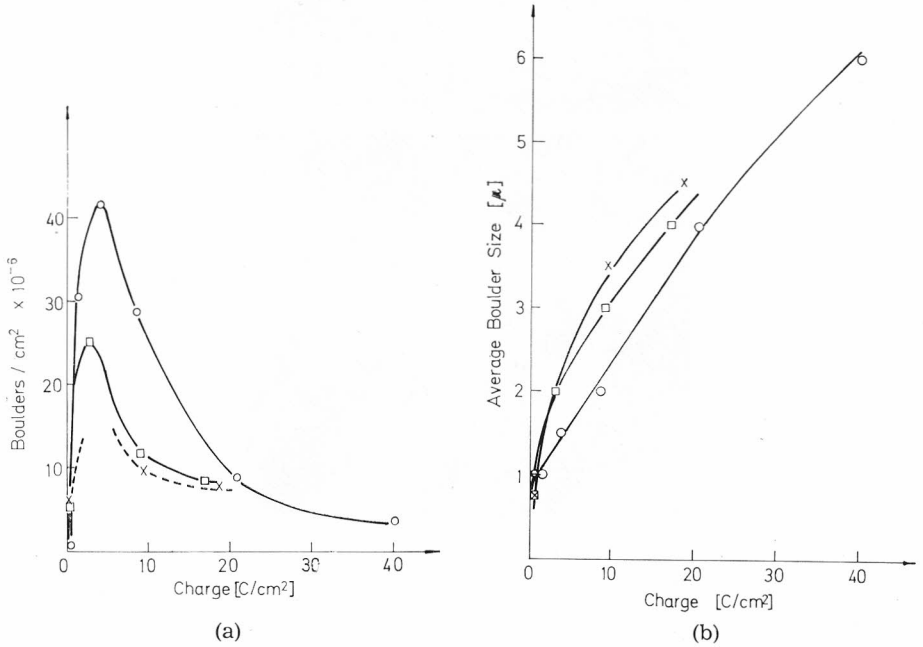

Fig. 13. *a*) Boulder density as function of charge. X — electrode No. 1; 0 — electrode No. 2; □ — electrode No. 3.

b) Average boulder size as function of charge. X — electrode No. 1; 0 — electrode No. 2; □ — electrode No. 3.

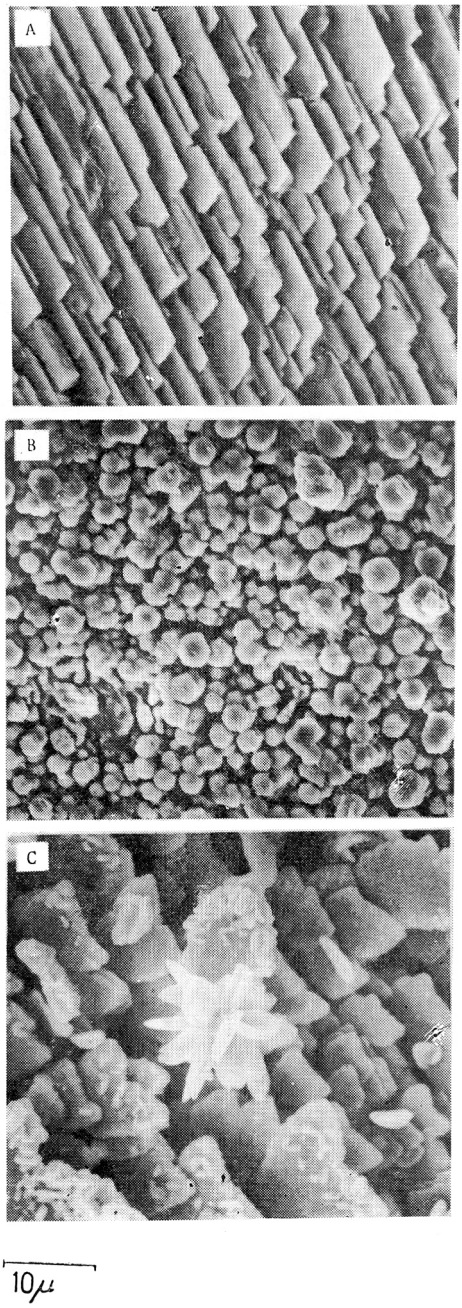

Fig. 14. SEM pictures of deposition from 0.02 M zincate solution. Electrode No. 1: *A* — 50 mV, 17 C/cm²; *B* — 100 mV, 13 C/cm²; *C* — 200 mV, 13 C/cm².

[To face page 207]

In summing up the experimental data and the previous discussion, the mechanism of zinc deposition and dissolution in low acidity zinc sulfate solutions can be represented by the following scheme:

$$Zn \rightarrow Zn_{adion} \tag{7}$$

$$Zn_{adion} \rightleftharpoons Zn\,(I) + e \tag{8}$$

$$Zn\,(I) \rightarrow Zn\,(II) + e \tag{9}$$

where Zn(II) and Zn (I) represent the di-and mono-valent Zn particles, probably complexed or ion-paired with sulfate anions. The reaction is rate-controlled by step (9) while for higher Zn ion concentration the first, surface diffusion step (7) appears as the rate controlling too.

Electrocrystallization of Zinc from Alkaline Solutions and Morphology of the Deposit

The mechanism of zinc deposition from zincate solutions has been studied extensively, and the recent work[2] suggests the following reaction sequence

$$Zn\,(OH)_4^{2-} \rightleftharpoons Zn\,(OH)_3^- + OH^- \tag{10}$$

$$Zn\,(OH)_3^- + e \rightarrow Zn\,(OH)_2^- + OH^- \tag{11}$$

$$Zn\,(OH)_2^- \rightleftharpoons Zn\,(OH) + OH^- \tag{12}$$

$$ZnOH + e \rightleftharpoons Zn + OH^- \tag{13}$$

However, the understanding of the mechanism of the charge transfer reaction still does not answer the important practical question why the morphology of the deposited zinc varies from the smooth, layer-type growth to the mossy, dendrytic or even powder type, all depending on the experimental conditions of the deposition. The known experimental facts are that layer type and mossy deposit is obtained at lower overpotentials, while the increase of overpotential favours the dendrytic growth or even powder formation. Despić and Diggle proposed a theory of dendrytic growth[19] developed later in more detail[20], starting with the assumption that if the zinc deposition is under diffusion controlled conditions the thickness of the effective diffusion layer is different over the rough metal surface. If the roughness is of the same order of magnitude as the thickness of the diffusion layer, the peak points will have a thinner diffusion layer than the other parts of the surface, and hence will grow faster than the rest of the surface. The result is the dendrite formation. This theory was experimentally verified[21], and seems to be a satisfactory one.

It has, however, still to be answered why the initially smooth zinc surface becomes rough during the deposition, with the formation of the precursors of dendrites, and why this happens only under certain experimental conditions.

In the attempt to answer these questions in a series of experiments (for details* see the original paper[18]). The morphology of the zinc deposit was observed under the scanning electron microscope as the function of the charge used for potentiostatic deposition at 50, 100 and 200 mV of overpotential. As the substrate for deposition a 3 mm zinc rod with large crystallites (obtained by long annealing), was used, with the orientation of the electro-polished cry-

* This part of the work was done by Dr. Nagy as a part of his Ph. D. thesis in the Electrochemistry Laboratory, University of Pennsylvania, Philadelphia.

stallite surface determined by a separate X-ray analysis. Hence, the crystallographic orientation of the deposited zinc could be determined as well. Since the concentration of zincate ions was rather low, (the electrolyte was 2 M KOH + 0.1 M zincate), the limiting diffusion current was achived already at 100 mV of cathodic overpotential.

The deposit obtained at 50 mV was of the layer type, with the occasional appearance of boulders even though the apparent appearance of the deposit varied from sample to sample as shown in Fig. 7. The most illustrative is case D of the three crystallite boundaries with the different orientation of each crystallite and different appearance of the deposit. However, if the known »c« axis of the substrate crystallite is aligned with the optical axis of the microscope, *i. e.*, each surface is viewed under the same angle, the difference in appearances disappears, as shown in Fig.8, indicating in both cases layer-type growth.

From the interrupted deposition experiments and subsequent microscopic observation the widening of the layer steps with time of deposition was observed. The relation between the average layer width and the thickness of the deposit expressed as C/cm^2 is given in Fig. 9 for two sets of experiments indicating the linearity of this relationship.

The deposition at 100 mV produced a deposit consisting of boulders. The first boulders were observed after 10—15 seconds of deposition, and they appeared in increasing numbers till the surface was completely covered, then their number decreased. The size of the boulders continually increased during the course of deposition. A typical photographed series is shown in Fig. 10. There is a tendency for the boulders to segregate at grain boundaries of the original substrate, as shown in Fig. 11 for deposition, dissolution and redeposition experiments.

Photographs taken with the »c« axis of the crystal aligned with the optical axis of the microscope (Fig 12) reveal that not all of the boulders are epitaxial with the substrate, but some of them are misaligned (encircled boulders).

From the series of interrupted depositions with the subsequent microscopic observations, the variation of average boulder density and size was determined as a function of deposition thickness and shown in Figs. 13a and b. After the initial sharp increase of the number of boulders it reaches a peak and then decreases as the size of the remaining boulders becomes larger and larger, and the surface rougher and rougher.

The origin of the boulders could be either points of already existing screw dislocations or could be formed by the nucleation of adions. A distinction between the two mechanisms of boulder growth can be obtained from the crystallographic orientation of the boulders relative to the substrate. If growth originates from screw dislocations complete epitaxy is expected, whilst some deviation from epitaxy can arise if the boulders are nucleated. The preferred orientation of the nucleated boulders will be that of substrate, since the epitaxial nucleation energy is less than that of the nonepitaxial,but the appearance of some nonepitaxial nuclei can occur. As shown in Fig. 12 this is the real case. Hence, it can be concluded that deposition at 50 mV proceeds via the layer type of growth, the overpotential not being large enough to form stable nuclei at the flat portions of the layer steps. At 100 mV deposition proceeds initially *via* the layer growth with the fast step widening until the sufficient stepwidth and surface adion concentration is achieved for the nucleus formation.

For the roughening of the surface the following model was proposed. The boulders are nucleated progressively with a constant rate v (boulders/cm^2 sec). Since the boulders are grown under the diffusional control the current into a particular boulder is proportional to its cross sectional area, when the surface is already covered with boulders. If as a first approximation the boulders are considered as hemispheres with the radius r, the current into one boulder at the total current density i is: $r^2 \pi i$. If a is the volume of material in cm^3/sec, deposited by each mA/cm^2, the change of volume of a boulder with time is

$$\frac{dV}{dt} = i a r^2 \pi \tag{14}$$

The volume of a boulder is

$$V = \frac{2\pi}{3} r^3 \tag{15}$$

and

$$dV = 2\pi r^2 dr \tag{16}$$

Substituting (16) into (14) gives

$$\frac{dr}{dt} = \frac{1}{2} i a \tag{17}$$

or upon integration

$$r = \frac{1}{2} i a t \tag{18}$$

Hence, the rate of increase of the radius of the boulder is independent of the size of the boulder. The final consequence of this fact is that small boulders will be consumed by the larger ones when they meet at the surface. It can be shown on the basis of the given model that the number of boulders should be related by the following relation to the time of deposition

$$N = vt \exp(-\pi/24\, i^2 a^2 v t^3) \tag{19}$$

This equation describes the curves of Fig. 13a with a reasonable agreement. It predicts a nearly linear rise while the size of the boulders is small and a maximum at 5 C/cm^2 ($\tau = 350$ sec) and $N = 34 \times 10^6$ boulders/cm^2 (calculated with $v = 1.4 \times 10^5$ boulders/cm^2 sec, taken from the initial slope of curves on Fig. 13a. This agreement between the observed and calculated number of boulders gives support to the proposed model of roughening consisting of continous nucleation and the consumption of smaller boulders by the larger ones.

After the longer deposition process it can be expected that some of the boulders will become large enough, or in other words the surface rough enough, for the differences of diffusion layer thickness to start accelerating the growth of the largest particles into dendrites according to the dendrite growth theory of Despić *et al.*

In a separate set of similar experiments in which only the concentration of zincate ions was reduced to 0.01 M, and hence the limiting diffusion current, *i. e.* the deposition current reduced by 10 times, the same morphology of the deposit was obtained at 50 and 100 mV, as shown in Fig. 14. For the same amount of material deposited at 200 mV even larger boulders were obtained and already a dendrite appeared, supporting the suggested model of roughening and dendritic growth. Another important conclusion which obtained clear

proof is that it is the overpotential of deposition which determines the morphology of the deposit and not the used current density as assumed by some authors[22].

REFERENCES

1. D. Jovanović, *Ph. D. Thesis*, University of Belgrade, Belgrade 1972.
2. J. O'M. Bockris, Z. Nagy, and A. Damjanović, *J. Electrochem. Soc.* **119** (1972) 3.
3. V. I. Kravcov and G. V. Zverevich, *Vestn. Leningr. Univ.* **16** (1963) 103.
4. V. V. Losev and G. M. Budev, *Zhur. Fiz. Khim.* **37** (1963) 842, 1230, 1461.
5. W. Lorenz, *Z. Phys. Chem. N.F.* 19 (1959) 377.
6. M. V. Zvereva and A. L. Rotinjan, **39** (1966) 1979, 2254.
7. T. Hurlen, *Acta Chem. Scand.* **6** (1962) 1337.
8. J. O'M. Bockris, D. M. Dražić, and A. R. Despić, *Electrochim. Acta* **4** (1961) 325.
9. D. M. Dražić, S. Djordjević, and M. Vojnović, *XX CITCE Meeting*, Strassbourg, 1969.
10. D. M. Dražić and S. Hadži Jordanov, *Proc. XV Meeting of Chemist of SR Serbia*, Novi Sad 1970, Bull. Chem. Soc. Belgrade **35** (1970) 166.
11. D. M. Dražić and S. Hadži Jordanov, *Bull. Chem. Soc.* Belgrade (in press)
12. A. R. Despić and J. O'M. Bockris, *J. Chem. Phys.* **32** (1960) 389.
13. W. Mehl and J. O'M. Bockris, *J. Chem. Phys.* **27** (1957) 818.
14. Landolt-Börnstein, *Physikalisch-Chemische Tabellen*, IV Ed. 1912, p. 1132.
15. G. H. Nanocollas, *Interactions in Electrolyte Solutions*, Elsevier Publ. Co., Amsterdam, 1966, p. 21.
16. J. O'M. Bockris and A. K. N. Reddy, *Modern Electrochemistry*, MacDonald, London, 1970, p. 876.
17. *ibid*, p. 1007.
18. J. O'M. Bockris, Z. Nagy, and D. M. Dražić, *J. Electrochem. Soc.* **120** (1973) 30.
19. A. R. Despić, J. W. Diggle, and J. O'M. Bockris, *J. Electrochem. Soc.* **115** (1968) 507.
20. J. W. Digle, A. R. Despić, and J. O'M. Bockris, *J. Electrochem. Soc.* **116** (1969) 1503.
21. A. R. Despić and M. M. Purenović, *J. Chem. Phys.* (submitted for publication)
22. F. Mansfeld and S. Gilman, *J. Electrochem. Soc.* **117** (1970) 588.

IZVOD

Elektrokristalizacija metala. Ispitivanje cinka

D. M. Dražić, S. Hadži Jordanov i Z. Nagy

U zavisnosti od uslova pri kojima se vrši elektrodepozicija cinka mogu se zapaziti različiti efekti na proces elektrokristalizacije.

U kiselim rastvorima cink-sulfata, pri manjim vrednostima ukupne prenapetosti, javlja se i znatna prenapetost izazvana površinskom difuzijom, ukazujući da je spori stupanj reakcije taloženja površinska difuzija adjona. Neobična zavisnost struje izmene od pH sa minimumom kod pH ~ 2 ukazuje na verovatnu promenu strukture reagujuće čestice kod ovog pH. Predložen je i mehanizam elektrohemijske reakcije.

U alkalnim rastvorima nisu zapaženi efekti površinske difuzije. Međutim, morfologija cinkovog depozita, koji se zbog male rastvorljivosti cinkata većinom taloži uz znatnu koncentracionu prenapetost, zavisi od elektrodnog potencijala. Ovo se uočava kod eksperimenata u kojima je morfologija depozita dobijenog pri raznim prenapetostima posmatranjem na elektronskom mikroskopu sa pokretnim zrakom *(scanning electron microscope)*, pri čemu je pokazano da je mogućno prekidanje i nastavljanje rasta depozita posle mikroskopskog posmatranja.

Pri malim prenapetostima (do 50 mV) dobija se epitaksijalni rast u slojevima koji linearno povećavaju širinu mikrosloja sa vremenom taloženja. Predloženo je teorijsko objašnjenje zapaženih efekata kristalografske orijentacije supstrata.

Pri većim prenapetostima (50—100 mV) dobija se depozit izgleda rasutog kamenja, pri čemu deo ovih izraslina nije epitaksijalan u odnosu na supstrat. Pretpostavlja se da su izrasline nastale nukleacijom. Broj izraslina po jedinici površine s vremenom taloženja prvo naglo raste, a zatim lagano opada. Statistička analiza ovog fenomena, pretpostavljajući model da tokom rasta veće izrasline prekrivaju male, u saglasnosti je sa eksperimentom.

Produženim taloženjem izvestan broj izraslina na formiranoj rapavoj površini prerasta u dendrite.

TEHNOLOŠKO-METALURŠKI FAKULTET
UNIVERZITET U BEOGRADU
11000 BEOGRAD

Primljeno 11. decembra 1972.